

Numerical Study of Coupled Non-Gray Radiation and Separation Convection Flow in a Duct using FSK Method

M. Atashafrooz*

Department of Mechanical Engineering,
Sirjan University of Technology, Sirjan, Iran
E-mail: m.atashafrooz@sirjantech.ac.ir,
*Corresponding author

S. A. Gandjalikhan Nassab

Department of Mechanical Engineering,
Shahid Bahonar University of Kerman, Kerman, Iran
E-mail: ganj110@uk.ac.ir

K. Lari

Department of Mechanical Engineering,
Graduate University of Advanced Technology, Kerman, Iran
E-mail: k.lari@ymail.com

Received: 3 July 2016, Revised: 15 October 2016, Accepted: 23 October 2016

Abstract: In this research, the coupling between non-gray radiation and separation convection flow in a duct is investigated numerically. Distributions of absorption coefficients across the spectrum ($50\text{cm}^{-1} < \eta < 20000\text{cm}^{-1}$) are obtained from the HITRAN2008 database. The full-spectrum k-distribution method is used to deal with the non-gray part of the problem, while the gray radiation calculations are performed using the Planck mean absorption coefficient. To find the divergence of radiative heat flux distribution, the radiative transfer equation (RTE) is solved by the discrete ordinates method (DOM). The effects of radiation-conduction parameter, scattering coefficient and wall emissivity on thermal behaviors are investigated for both gray and non-gray mediums. In addition, the results of gray medium are compared with non-gray results as a real case. The results show that in many cases, use of gray simulations is not acceptable and leads to significant errors, especially in non-scattering medium with high values of radiation-conduction parameter and wall emissivity.

Keywords: Backward facing step, Combined convection-radiation, DOM, FSK method, Non-gray medium, Separation flow

Reference: Atashafrooz, M., Gandjalikhan Nassab, S. A., and Lari, K., "Numerical study of Coupled Non-Gray Radiation and Separation Convection flow in a Duct Using the FSK Method", Int J of Advanced Design and Manufacturing Technology, Vol. 9/No. 4, 2016, pp. 23-38.

Biographical notes: **M. Atashafrooz** is an assistant professor in the Sirjan University of Technology, Sirjan, Iran. He received his PhD from Shahid Bahonar University of Kerman in 2015. He has several published papers about radiation heat transfer. **S. A. Gandjalikhan Nassab** is a professor in the Shahid Bahonar University, Kerman, Iran. He has several published papers about radiation heat transfer and also in the CFD research area. **K. Lari** is an assistant professor in the Graduate University of Advanced Technology, Kerman, Iran. He received his PhD from Shahid Bahonar University of Kerman in 2011. He has several published papers about radiation heat transfer.

1 INTRODUCTION

Separation flow accompanied with heat transfer has received continuous attention during new decades because of its important influence in the design of many engineering applications, such as power generating equipments, cooling of electronic systems, heat exchangers, gas turbine blades and combustion chambers. Backward facing step (BFS) is one of the most fundamental geometries where the flow over them has the most features of separated flows. BFS is known as a benchmark problem and there are many published works about separated convection flow over this geometry by several investigators [1-6]. Among previous works, Nie et al., [7], Tsay et al., [8], and Chen et al., [9] studied BFS to examine effects of baffle and step inclination angle on flow and heat transfer distributions. In other researches, investigations of entropy generation in laminar forced convection flow in channels with expansion or contraction were studied by Abu-Nada [10] and Atashafrooz et al., [11-12]. More recently, at different points of view, this geometry has been investigated by Selimefendigil and Oztop [13-14].

In some of the mentioned applications, besides the convective and conductive heat transfer, radiative heat transfer also plays an important role on thermal behaviors. When radiation and convection effects are of similar importance, separate calculation of those and superposition without considering their interaction lead to significant errors. Therefore, in order to accurately determine the temperature field and heat transfer rates in such engineering applications, the flowing fluid must be considered as a radiating medium and energy equation should be contained all of the heat transfer mechanisms including convection, conduction and radiation. In the coupled convection and radiation problems, when the flowing gas behaves as a participating medium, its complex absorption, emission and scattering introduce a considerable difficulty in the simulation of these flows.

Often in calculations of combined convection and radiation heat transfer, the participating gases are assumed to be gray hence there is no spectral dependence on the radiative properties [15-18]. This is essentially done to reduce the computation time to solve the radiative transfer equation (RTE). Among the works with gray medium assumption, Ko and Anand [19] studied three-dimensional combined convective-radiative heat transfer over a backward-facing step using a finite volume method (FVM). In that work, a detailed analysis for the distribution of reattachment length, bulk temperature, and Nusselt number was carried out to investigate the effects of radiation on fluid flow and heat transfer. Simulations of laminar forced convection flow of a radiating gas over an

inclined backward facing step in a duct under different condition were presented by Ansari and Gandjalikhan Nassab [20] and the present authors [21-22]. The results of those works show that the radiative parameters have great effects on the thermal behaviours of the convective flow. In addition, the present authors [23-24] studied numerical analysis of combined convection-radiation heat transfer over a recess including two inclined backward and forward facing steps in a horizontal duct. In those studies, the Cartesian coordinate system was used to simulate the inclined surfaces by considering the blocked-off region in regular grid.

The radiative properties of many participating gases, such as CO₂ and H₂O, are dependent on the wavelength. These properties vary strongly and rapidly across the spectrum. Hence, in order to analyze all effects of the radiation on the problems, the medium should be considered as non-gray and the radiative heat transfer should be modeled using the spectral models. In fact, this approach leads to a high accuracy in calculations of radiative heat transfer problems. Several spectral models have been developed to account for the non-gray behavior introduced by the spectral variation of the gases' radiative properties.

These models can broadly be grouped into three categories; line-by-line (LBL) model, spectral band model, and global model (full spectrum model). Line-by-line models are based directly on spectroscopic databases and are the most accurate method for simulation of the non-gray medium. In these models, for calculating the radiative properties of participating gases (mainly H₂O, CO₂, and soot), thousands of lines and thousands of bands across the spectrum are needed [25-26]. Therefore, LBL models require large computer resources and computational time, and fail to be a feasible method for engineering applications, especially in the case of coupled heat transfer modes.

Band models are divided into several popular sub models such as narrow band model (NBM) [27], wide band model (WBM) [28-29] and more recently developments such as the statistical narrow band correlated-k (SNBCK) [30] and narrow band k-distribution methods [31]. Narrow band model (NBM) has a high accuracy and require a large number of bands and excessive computing time, whereas the wide band model (WBM) is less accurate and more economical. Also, the statistical narrow band correlated-k method (SNBCK) is reasonably accurate and suitable for practical spectral radiation applications. Among the band models, NBM and WBM are difficult to be coupled to the solution methods of the RTE, such as DOM and FVM. But, the SNBCK and narrow band k-distribution methods are relatively easy to couple to DOM or FVM techniques. Global models (full spectrum models) are another set of

spectral models which have the lowest computation time among all the models and include several methods such as the spectral line-based weighted sum of gray-gases method (SLW) [32-33], the full-spectrum k-distribution method (FSK) [31], [34] and the absorption distribution function method (ADF) [35]. These models supply accurate results for modelling the radiative properties of real gases, such as CO₂ and H₂O, and are often the preferred choice if non-gray gas modelling is undertaken in CFD [36-37].

Among the full spectrum models, the full spectrum k-distribution method (FSK) is newest. This model has the ability to achieve high accuracy for homogeneous media at a tiny fraction of line-by-line's (LBL) computational cost [34]. In fact, this method has been derived from an approach based on narrow band k-distributions and is easy to be coupled to the solution methods of the RTE. More details of this method are explained in "Full-Spectrum k-Distribution (FSK) Method" section. Since the FSK method is new, it is still under development [38-39]. There are a few numbers of literatures in the area of coupled radiation and convection problems using FSK method. Porter et al., [40] used this method to study the radiative heat transfer in gaseous oxy-fuel combustion environments. In one of the latest researches, numerical study of non-gray radiation and natural convection using the FSK method is done by Lari et al., [41]. The aim of that work was to analyze the thermal and flow behaviors of real cases with a small temperature difference.

To the best of the authors' knowledge, the coupling between non-gray radiation and forced convection flow over an inclined backward facing step, which provides separated flows, is still not studied. This motivates the present study, which the interaction of non-gray radiation and forced convection on thermal behaviours of the step flow is investigated here for the first time. In fact, the aim of this work is to analyze the thermal behaviours of laminar forced convection flow of a radiating gas over an inclined BFS for different medium assumptions such as pure convection, gray medium and non gray medium. Also, gray radiation calculations are compared with non-gray results as a real case to obtain the error rate of gray medium assumption in engineering applications. Since, the full spectrum k-distribution is an effective non-gray radiation model, this model is used to handle the non-gray part of the problem, while the RTE is solved using the conventional DOM.

2 PROBLEM DESCRIPTION

The geometric model used in this research (Figure 1) is an inclined backward facing step in a horizontal duct. According to Figure 1, the x and y symbols denote the

horizontal and vertical coordinates. The step inclination angle is considered $\phi = 60^\circ$ which is evaluated from the horizontal sense. The upstream and downstream heights of the duct are depicted as h and H, respectively, such that the expansion ratio ($ER=H/h$) of this geometry is equal to 2. The total length of the duct is considered to be 23H, whereas the ratio of the upstream length to downstream height is $L_1/H=3$ and the downstream length is equal to $L_2=20H$. This is made to ensure that the flows at the inlet and outlet sections are not affected significantly by the sudden changes in the geometry and flow at the exit section becomes fully developed.

The no-slip condition is used on the solid surfaces. The temperature on the step surfaces and the bottom wall is kept at T_h and the top wall temperature is T_c , which is assumed to be lower than T_h . At the inlet duct section, the air mixture flow is fully developed with uniform temperature of $T_{in}=T_c$. At the outlet section, zero axial gradients for velocity components and temperature of fluid are applied. Also, the walls are assumed to emit and reflect diffusely with constant wall emissivity.

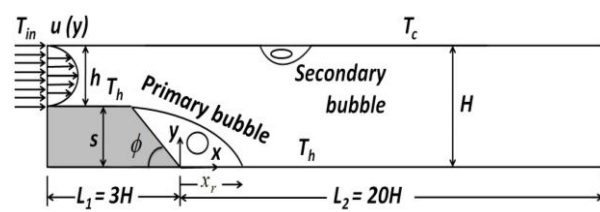


Fig. 1 Schematic of problem geometry

It should be mentioned that the air in the duct is considered a mixture of two absorbing gases, CO₂ and H₂O with 10% and 20% mole fractions, respectively. Also, this participating medium can be gray or non-gray depending on the applied assumption.

3 GOVERNING EQUATIONS

For combined convection and radiation heat transfer, the energy equation can be written as follow:

$$u \frac{\partial T}{\partial x} + v \frac{\partial T}{\partial y} = \alpha \left(\frac{\partial^2 T}{\partial x^2} + \frac{\partial^2 T}{\partial y^2} \right) - \frac{1}{\rho c_p} \nabla \cdot \vec{q}_r \quad (1)$$

In this equation, u and v are the velocity components in x- and y- directions, respectively, and can be calculated by the continuity and momentum equations:

$$\frac{\partial u}{\partial x} + \frac{\partial v}{\partial y} = 0 \quad (2)$$

$$u \frac{\partial u}{\partial x} + v \frac{\partial u}{\partial y} = -\frac{1}{\rho} \frac{\partial p}{\partial x} + \frac{\mu}{\rho} \left(\frac{\partial^2 u}{\partial x^2} + \frac{\partial^2 u}{\partial y^2} \right) \quad (3)$$

$$u \frac{\partial v}{\partial x} + v \frac{\partial v}{\partial y} = -\frac{1}{\rho} \frac{\partial p}{\partial y} + \frac{\mu}{\rho} \left(\frac{\partial^2 v}{\partial x^2} + \frac{\partial^2 v}{\partial y^2} \right) \quad (4)$$

It should be mentioned that the above equations are expressed for steady two-dimensional laminar incompressible flow. In these equations, physical and thermal properties of air mixture are considered constant. Furthermore, the final term on the right-hand side of the energy equation is the divergence of the radiative heat flux ($\nabla \cdot \vec{q}_r$) that is computed in the next sections.

3.1. Gas Radiation Modelling

As it is seen from energy equation, the divergence of the radiative heat flux ($\nabla \cdot \vec{q}_r$) is required to calculate the radiative term in this equation. This term per unit wavenumber at a certain spectral position can be computed as follow [34]:

$$\nabla \cdot \vec{q}_{r\eta} = \sigma_{a\eta} \left(4\pi I_{b\eta}(\vec{r}) - \int_{4\pi} I_{\eta}(\vec{r}, \vec{s}) d\Omega \right) \quad (5)$$

To calculate the divergence of the total radiative heat flux, it should be integrated from $\nabla \cdot \vec{q}_{r\eta}$ over the spectrum:

$$\nabla \cdot \vec{q}_r = \int_0^{\infty} \sigma_{a\eta} \left(4\pi I_{b\eta}(\vec{r}) - \int_{4\pi} I_{\eta}(\vec{r}, \vec{s}) d\Omega \right) d\eta \quad (6)$$

In the above equation, $\sigma_{a\eta}$ is the spectral absorption coefficient of the gas, $I_{b\eta}(\vec{r})$ is the spectral black body emission at local temperature and $I_{\eta}(\vec{r}, \vec{s})$ is the spectral radiation intensity at the situation \vec{r} and in the direction \vec{s} . For calculation of $\nabla \cdot \vec{q}_r$, the spectral radiation intensity field is primary needed. To obtain this term, it is necessary to solve the RTE.

3.2. Radiative Transfer Equation

The radiative transfer equation in spectral form can be expressed as [34]:

$$\vec{s} \cdot \nabla I_{\eta}(\vec{r}, \vec{s}) = \sigma_{a\eta} I_{b\eta}(\vec{r}) - (\sigma_{a\eta} + \sigma_s) I_{\eta}(\vec{r}, \vec{s}) + \frac{\sigma_s}{4\pi} \int_{4\pi} I_{\eta}(\vec{r}, \vec{s}') \varphi(\vec{r}, \vec{s}, \vec{s}') d\Omega' \quad (7)$$

In which, σ_s and $\varphi(\vec{r}, \vec{s}, \vec{s}')$ are the scattering coefficient and the scattering phase function, respectively. In this paper, it is assumed that these parameters are independent of wavenumber (gray). In fact, the phase function is equal to unity because of the assumption of isotropic scattering behaviour of the participating gas.

The boundary condition for a diffusely emitting and reflecting surface is [34]:

$$I_{\eta}(\vec{r}_w, \vec{s}_i) = \varepsilon_w I_{b\eta}(\vec{r}_w) + \frac{(1 - \varepsilon_w)}{\pi} \int_{\vec{n}_w \cdot \vec{s}_j < 0} I_{\eta}(\vec{r}_w, \vec{s}_j) |\vec{n}_w \cdot \vec{s}_j| d\Omega' \quad \vec{n}_w \cdot \vec{s}_i > 0 \quad (8)$$

In this equation, $I_{b\eta}(\vec{r}_w)$ is the black body spectral radiation intensity at the temperature of the boundary surface, \vec{n}_w is the outward unit vector normal to the surface and ε_w is the wall emissivity. In addition, it is necessary to be noted that the inlet and outlet duct sections are considered as black walls at the fluid temperatures in inlet and outlet sections, respectively.

3.3. Full-Spectrum k-Distribution (FSK) Method

In this study, the full-spectrum k-distribution (FSK) method is used to account for non-gray radiative properties. As it is mentioned before, this method has the lowest computation time among all methods and thus is often the preferred choice if non-gray gas modelling is undertaken in CFD. The full-spectrum k-distribution demands that except for the absorption coefficient, no other radiative property varies across the spectrum. It should be mentioned that this approach is also valid for arbitrarily scattering media and for arbitrarily reflecting surfaces, as long as the absorption coefficient remains the only spectrally varying radiative property [31], [38]. However, by FSK method, RTE can be reordered in smoothly-varying g-space as [31], [34]:

$$\frac{dI_g(\vec{r}, \vec{s})}{ds} = \vec{s} \cdot \nabla I_g(\vec{r}, \vec{s}) = kI_b(\vec{r}) - (k + \sigma_s) I_g(\vec{r}, \vec{s}) + \frac{\sigma_s}{4\pi} \int_{4\pi} I_g(\vec{r}, \vec{s}') \varphi(\vec{r}, \vec{s}, \vec{s}') d\Omega' \quad (9)$$

With the boundary conditions

$$I_g(\vec{r}_w, \vec{s}_i) = \varepsilon_w a(T_w, T, g) I_b(\vec{r}_w) + \frac{(1 - \varepsilon_w)}{\pi} \int_{\vec{n}_w \cdot \vec{s}_j < 0} I_g(\vec{r}_w, \vec{s}_j) |\vec{n}_w \cdot \vec{s}_j| d\Omega' \quad \vec{n}_w \cdot \vec{s}_i > 0 \quad (10)$$

Where

$$I_g = \frac{\int_0^{\infty} I_{\eta} \delta(k - \sigma_{a\eta}) d\eta}{f(T, k)} \quad (11)$$

$$g(T, k) = \int_0^k f(T, k) dk \quad (12)$$

$$a(T_w, T, g) = \frac{f(T_w, k)}{f(T, k)} = \frac{dg_w(T_w, k)}{dg(T, k)} \quad (13)$$

And a full-spectrum k-distribution is defined as:

$$f(T, k) = \frac{1}{I_b} \int_0^{\infty} I_{b\eta} \delta(k - \sigma_{a\eta}) d\eta \quad (14)$$

In equations (9) to (14), I_g is the radiative intensity being solved in g-space, T is the temperature of the homogeneous medium and k is the reordered local absorption coefficient $\sigma_{a\eta}$ at temperature T for the Planck function weight. Also, I_b is the total black body intensity, $\delta(k - \sigma_{a\eta})$ is the Dirac-delta function, and $f(T, k)$ is a Planck-function-weighted k -distribution which is a function of temperature through the blackbody intensity. Moreover, g is the cumulative k -distribution and physically, it is the Planck-function-weighted fraction of the spectrum with absorption coefficient of $\sigma_{a\eta} < k$, and $a(T_w, T, g)$ is a non-gray stretching factor accounting for the difference of wall temperatures T_w from the temperature T in the Planck function that is used to construct the k - g distributions. The details of this method were described in the previous studies by Modest [31], [34] and Modest and Zhang [38]. Moreover, in order to obtain the divergence of the total radiative heat flux, equation (6) is rewritten into g -space as [31], [34]:

$$\nabla \cdot \vec{q}_r = \int_0^1 k \left(4\pi I_b - \int_{4\pi} I_g(\vec{s}) d\Omega \right) dg \tag{15}$$

Finally, the radiative heat flux at any arbitrary surface is calculated from the surface energy balance as [31], [34]:

$$\vec{q} \cdot n(r_w) = \varepsilon_w \left(\pi I_b(r_w) - \int_{\vec{n}_w \cdot \vec{s}' < 0} I(\vec{r}_w, \vec{s}') |\vec{n}_w \cdot \vec{s}'| d\Omega' \right) \tag{16}$$

Where, I is the total intensity and should be calculated from as following:

$$I = \int_0^\infty I_\eta d\eta = \int_0^1 I_g dg \tag{17}$$

It should be noted that the FSK method given by equations (9) to (17), has the ability to achieve LBL accuracy for homogeneous medium. Thus this method is suitable for the mediums with small temperature differences that can be considered homogenous ones. Also, it should be mentioned that this method can result in large errors in cases of large concentration gradients.

3.4. Discrete Ordinates Method (DOM)

The FSK's equation of radiation transport (equation (9)) is an integro-differential equation that can be solved using the discrete ordinates method. In the DOM, equation (9) is solved for a set of n different directions, \vec{s}_i , $i=1,2,3,\dots,n$ and integrals over solid angle are substituted by the numerical quadrature, that is,

$$\int_{4\pi} f(\vec{s}) d\Omega \cong \sum_{i=1}^n w_i f(\vec{s}_i) \tag{18}$$

Where w_i are the quadrature weights associated with the directions \vec{s}_i . According to this method, RTE is approximated by a set of n equations, as follows [34]:

$$\begin{aligned} (\vec{s}_i \cdot \nabla) I_g(\vec{r}, \vec{s}_i) &= k I_b(\vec{r}) - (k + \sigma_s) I_g(\vec{r}, \vec{s}_i) + \\ \frac{\sigma_s}{4\pi} \sum_{j=1}^n I_g(\vec{r}, \vec{s}_j) \phi(\vec{s}_j, \vec{s}_i) w_j & \quad i = 1, 2, 3, \dots, n \end{aligned} \tag{19}$$

Subjected to the boundary conditions:

$$\begin{aligned} I_g(\vec{r}_w, \vec{s}_i) &= \varepsilon_w I_b(\vec{r}_w) + \\ \frac{(1 - \varepsilon_w)}{\pi} \sum_{\vec{n}_w \cdot \vec{s}_j < 0} I_g(\vec{r}_w, \vec{s}_j) |\vec{n}_w \cdot \vec{s}_j| w_j & \quad \vec{n}_w \cdot \vec{s}_i > 0 \end{aligned} \tag{20}$$

More details of the numerical solution of RTE by DOM were described in the previous paper by the second author [42].

3.5. Gray Absorption Coefficient

In the present study, the gray radiation calculations are done using the Planck mean absorption coefficient. In fact, the Planck mean absorption coefficient is used as an averaged constant absorption coefficient in solving the gray radiation problems. This coefficient is obtained from line-by-line calculations using the following equation [34]:

$$k_p = \frac{\int_0^\infty I_{b\eta} \sigma_{a\eta} d\eta}{\int_0^\infty I_{b\eta} d\eta} = \frac{\pi}{\sigma T^4} \int_0^\infty I_{b\eta} \sigma_{a\eta} d\eta \tag{21}$$

3.6. The Main Physical Quantities

In this study, the following dimensionless parameters are used to describe the different behaviors of the solved problems:

$$\begin{aligned} (U, V) &= \left(\frac{u}{U_o}, \frac{v}{U_o} \right), \quad Re = \frac{\rho U_o H}{\mu}, \quad (X, Y) = \left(\frac{x}{H}, \frac{y}{H} \right), \\ \theta_2 &= \frac{T_h}{T_c}, \quad \Theta = \frac{T - T_c}{T_h - T_c}, \quad \theta_1 = \frac{T_c}{T_h - T_c}, \quad q_r^* = \frac{q_r}{\sigma T_h^4}, \\ RC &= \frac{\sigma T_h^3 H}{\kappa} \end{aligned} \tag{22}$$

The main physical quantities of interest in heat transfer study are the temperature field and Nusselt number distributions.

In laminar forced convection flow of a radiating gas, the energy transport from the duct wall to the gas flow depends on two related factors:

1. Fluid temperature gradient on the wall
2. Rate of radiative heat exchange on boundary surface

Therefore, total heat flux on the wall is the sum of convective and radiative heat fluxes such that $q_t = q_c + q_r = -k\left(\frac{\partial T}{\partial y}\right) + q_r$. The convective, radiative and total Nusselt numbers at the walls are calculated from these heat fluxes as follows [20-22]:
Convective Nusselt number:

$$Nu_c = \frac{q_c D_h}{\kappa(T_w - T_b)} = \frac{-l}{\Theta_w - \Theta_b} \frac{\partial \Theta}{\partial Y} \Big|_{Y=0} \quad (23)$$

Radiative Nusselt number:

$$Nu_r = \frac{q_r D_h}{\kappa(T_w - T_b)} = \frac{RC.\theta_1.\theta_2}{\Theta_w - \Theta_b} q_r^* \quad (24)$$

Total Nusselt number:

$$Nu_t = Nu_c + Nu_r = \frac{-l}{\Theta_w - \Theta_b} \frac{\partial \Theta}{\partial Y} \Big|_{Y=0} + \frac{RC.\theta_1.\theta_2}{\Theta_w - \Theta_b} q_r^* \quad (25)$$

In equations (23) to (25), Θ_b is the mean bulk temperature that can be calculated using the following equation:

$$\Theta_b = \frac{\int_0^l \Theta U dY}{\int_0^l U dY} \quad (26)$$

It should be considered that for pure convective hat transfer, total Nusselt number is equal to its convective part.

4 NUMERICAL SOLUTION PROCEDURE

The continuity, momentum and energy equations are discretized using the finite volume method by integrating over an elemental cell volume. The control volumes are located utilizing the staggered grid arrangement for the x- and y- velocity components, while other variables of interest are computed at the grid nodes. The discretized forms of the governing equations are numerically solved by the SIMPLE algorithm of Patankar and Spalding [43]. Numerical solutions are obtained iteratively by the line-by-line method.

In this research, the air in the duct is considered as a mixture of two absorbing gases, CO₂ and H₂O with 10% and 20% mole fractions, respectively. Therefore, for each species, distribution of the absorption

coefficient $\sigma_{a\eta}$ across the spectrum ($50\text{cm}^{-1} < \eta < 20000\text{cm}^{-1}$) is obtained from meticulous line-by-line computations based on the HITRAN2008 database [44]. In fact, variable mixtures of different absorbing gases create no additional difficulty because the absorption coefficient of all species can simply be added up [34]. Then, according to this subject, the absorption coefficients distributions of air mixture are calculated by summing up the absorption coefficients of all species. In order to have a clear view of these rigorous computations, distribution of absorption coefficient across the spectrum for air mixture with 10%CO₂ and 20%H₂O is shown in Figure 2. As it is seen from this figure, the absorption coefficient varies so strongly along the full range of spectrum.

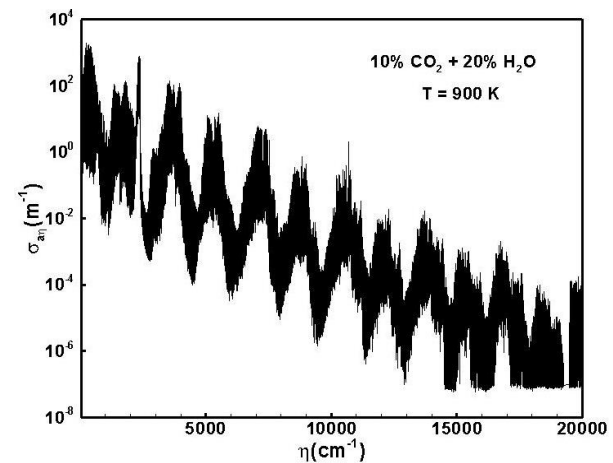


Fig. 2 Distribution of absorption coefficient across the spectrum for air mixture with 10% CO₂ and 20% H₂O

For gray radiation calculations, this distribution of line-by-line absorption coefficient is utilized with Eq. (21) to evaluate mean absorption coefficient k_p . Then, k_p is used instead of k in Eq. (9), and the RTE is solved only once for each direction.

In non-gray computations, using the obtained line-by-line absorption coefficient distribution, the cumulative k-distribution $g(T, k)$ and weight function $a(T_w, T, g)$ are obtained from Eqs. (12) to (14) using T_{ave} instead of the temperature of homogeneous medium (T) (details are described in Refs. [31], [34]). By this process, the rapidly oscillating absorption coefficient distribution $\sigma_{a\eta}$ converts to a smooth distribution of k which is a function of non-dimensional wavenumber (artificial wavenumber) g . In order to have a clear view of generating the full-spectrum k-distribution, the cumulative k-distribution $g(T, k)$ and weight function $a(T_w, T, g)$ for air mixture with 10%CO₂ and 20%H₂O are shown in Fig. 3.

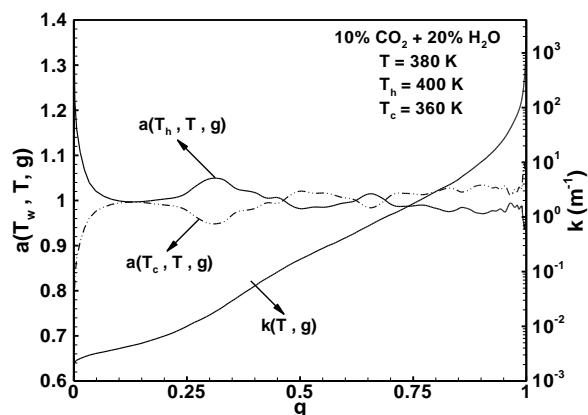


Fig. 3 k-g distribution and weight function for air mixture with 10% CO₂ and 20% H₂O at T=380 K

Since the k distribution is smooth, thus it can be approximated with an appropriate N-point numerical quadrature scheme. In this work, 12-point, third order Gaussian quadrature of moments is utilized to obtain the quadrature points for approximating k - g distribution. In addition, in order to obtain $\nabla \cdot \vec{q}_r$ that is needed for the numerical solution of the energy equation, the reordered RTE (equation 9) is solved for all quadrature points in each direction by DOM. Since, in the DOM, different numbers of discrete directions can be chosen during S_N approximation, the results obtained by the S_4 , S_6 , and S_8 approximations were compared and there was a small difference, less than 1% error, between S_6 and S_8 approximations. Therefore, S_6 approximation has been used in subsequent computations.

Also, it should be noted that to simulate the inclined surface, the blocked off method is employed for both radiation and convection problems (details are described in Refs. [20], [24], [45-46]). The solution technique can be summarized as follows:

- 1- A first approximation for the variables u , v , p and T at each node point is assumed.
- 2- The u - and v - velocity components are calculated from the momentum equations in the x - and y -directions.
- 3- Pressure field is computed according to the SIMPLE algorithm.
- 4- The RTE is solved to obtain the radiant intensity distribution. Then, the radiative source term in the energy equation is computed at each nodal point.
- 5- The temperature field inside the radiating medium is calculated from the energy equation.
- 6- Steps 2-5 are repeated until convergence is obtained.

About the convergence, it should be mentioned that the iterative process continues until achieving convergence of all dependent variables (velocity, pressure, temperature, and radiation intensity). For Navier-

Stokes and energy equations, the convergence of solution is evaluated using a criterion taken as the values of absolute residuals in these equations which become less than 10^{-4} , and the normalized errors in the velocity and temperature fields for each node satisfy the following criteria:

$$Error\Phi = \text{Max} \left| \frac{\Phi^n(i, j) - \Phi^{n-1}(i, j)}{\Phi^n(i, j)} \right| \leq 10^{-5}$$

Where, Φ denotes to all depending variables and n is the iteration level. But in the numerical solution of RTE, the maximum difference between the radiative intensities computed during two consecutive iteration levels did not exceed 10^{-6} at each nodal point for the converged solution. By this numerical strategy, the velocity, temperature, and radiation intensity distributions inside the flow domain can be obtained.

Table 1 Grid independence study, $RC=35$, $\sigma_s = k_p$, $\phi = 60^\circ$, $Re=500$

Grid size	\overline{Nu}_t	\overline{Nu}_t
	For gray medium	for non- gray medium
280×25	49.65	55.75
350×30	54.05	59.10
420×34	56.65	62.45
480×38	58.10	64.37
540×42	58.45	64.80

Based on the result of grid tests, to obtain the grid-independent solutions, several different meshes were used in the grid independence study. The corresponding value of average total Nusselt number along the bottom wall for gray and non-gray medium situations are calculated and tabulated in Table 1. As it is shown in Table 1, the grid size of 480×38 can be chosen for obtaining the grid independent solution, such that the subsequent numerical calculations are made based on this grid size. It should be mentioned that the grid is concentrated close to duct walls and near to the step corner in the x - and y - directions for obtaining more accuracy in the numerical calculations.

Table 2. The computation times, $RC=35$, $\phi = 60^\circ$, $Re=500$

Case problem	Pure convection	Gray medium	Non-gray medium
CPU time (min)	16	27	44

Finally, in order to have a view of calculation times in solving the set of governing equations with a FORTRAN computer code, CPU time for three medium situations are presented in Table 2. It should be noted that all computations are carried out using a personal computer: Intel (R) Core(TM) i5, CPU 2.53GHz and 4.00GB of RAM.

5 CODE VALIDATION

To validate the numerical solutions, several case problems have been solved as follows:

5.1. Validation of Fluid Flow

To verify the accuracy of computations in obtaining the flow characteristics, the results of reattachment point in flow over BFS and for different Reynolds numbers are compared with the experimental data [1] and numerical result [5] in Figure 4 and Table 3, respectively.

Table 3 Comparison of the computed reattachment point ($\frac{x_r}{s}$) with numerical findings in Ref. [5], $\phi = 90^\circ$

$Re = \frac{\rho U_0 H}{\mu}$	Erturk [5]	Current work
100	2.922	2.90
200	4.982	4.95
300	6.751	6.71
400	8.237	8.19
500	9.420	9.31

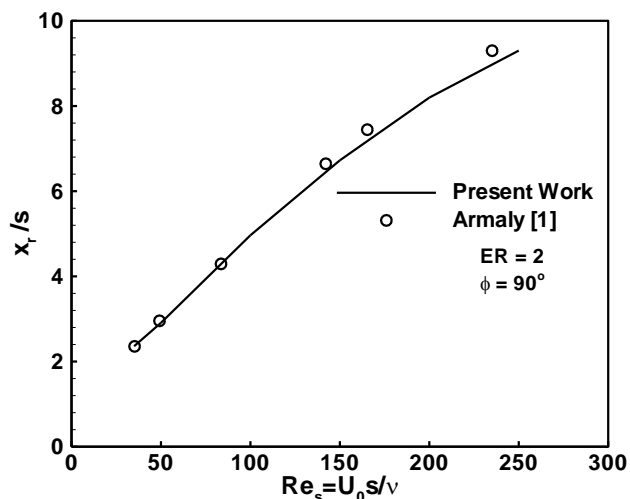


Fig. 4 Comparison of the computed reattachment point with experimental data [1]

As it is seen from Table 3 and Figure 4, the reattachment point moves toward the downstream side as the Reynolds number increases. However, a good agreement is seen between the present numerical results with those reported in literatures.

5.2. Validation of Combined Convection-Radiation Heat Transfer

As it was mentioned before, there are not any theoretical and experimental results about the coupling between non-gray radiation and forced convection flow over a BFS in a duct. But there is a research work about the laminar forced convection flow of a radiating gas over an inclined BFS with considering gray medium assumption done by Ansari and Gandjalikhan Nassab [21].

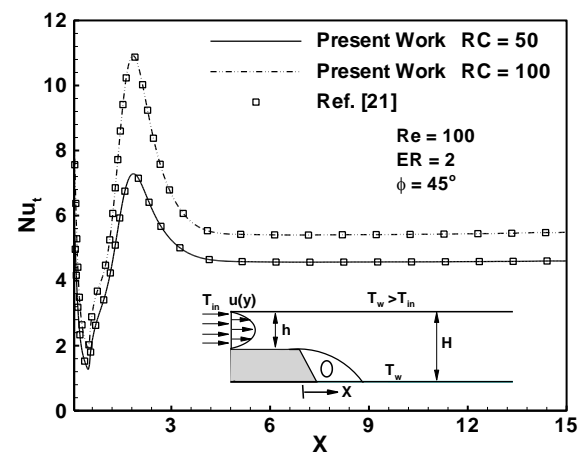


Fig. 5 Comparison of the computed total Nusselt number distribution along the bottom wall with theoretical findings in Ref. [21]

Therefore, to compare the results of combined convection–radiation heat transfer using DOM and blocked off method, another test case is studied based on the results of Ref. [21]. Distributions of total Nusselt number along the bottom wall at different values of the RC parameter are compared with those reported in Ref. [21]. Results are presented graphically in Figure 5. This Figure illustrates that the total Nusselt number increases by increasing in RC parameter. As it is seen from Figure 5, the results obtained in this study are in good agreement with findings in Ref. [21].

5.3. Validation of FSK Method

The accuracy of the results obtained by the FSK method is verified along a test case in which, a square enclosure is considered with length $L=1\text{m}$ containing homogenous and isothermal air at $T=380\text{K}$ with 10% CO_2 and 20% H_2O mole fractions. The bottom wall is hot at $T_h=400\text{K}$ and the top wall is cold at $T_c=360\text{K}$. The other walls are at $T=380\text{K}$ and all walls are black.

Only radiative heat transfer is considered in medium. The S_4 approximation is used to calculate radiant intensity and the spatial grid of 21×21 is used in the x- and y-directions, respectively. Distribution of non-dimensional radiative heat flux along the bottom wall is shown in Figure 6. These results are obtained by the LBL method using 1 million lines of absorption coefficient from the HITRAN 2008 database [44], and the FSK method using 500 and 12 quadrature points.

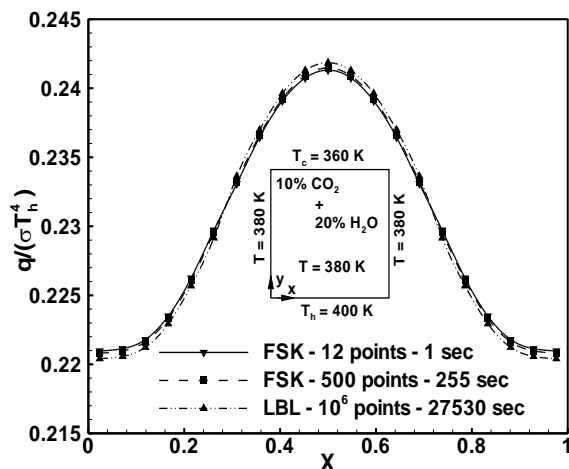


Fig. 6 Distribution of non-dimensional radiative heat flux Along the bottom wall obtained from the LBL and FSK methods

Figure 6 shows that the results obtained by FSK method for the homogenous and isothermal medium with low wall temperature differences are in good agreement with LBL results even with only 12 quadrature points. Although, according to computation times given in Figure 6, the FSK method is much faster than the LBL one. It should be noted that, in addition to the above validations, there are several other validations on these topics in the previous works by the second author [20], [41].

6 RESULTS AND DISCUSSION

The problem selected for this research is combined radiation and forced convection flow adjacent an inclined BFS in horizontal duct (Figure 1) containing air mixture with 10% CO_2 and 20% H_2O mole fractions. According to Figure 1, the temperature of hot and cold walls are considered $T_h = 400\text{K}$ and $T_c = 360\text{K}$, respectively. The air mixture is treated as an absorbing, emitting and scattering medium against thermal radiation. Due to the small range of temperature difference, the physical and thermal properties of the medium are considered to be constant and are evaluated at $T_{ave} = 380\text{K}$. In all subsequent numerical

calculations, the Reynolds number is considered to be 500. First, in order to obtain the flow pattern and better explanation of flow field, the streamlines are plotted in Figure 7. The effects of inclined step on the flow are clearly seen from the curvatures of streamlines. Figure 7 shows that two main recirculation zones are encountered for $\text{Re}=500$ in the flow domain. The primary recirculation region occurs downstream the step adjacent the bottom wall, whereas the secondary recirculation zone exists along the top wall.

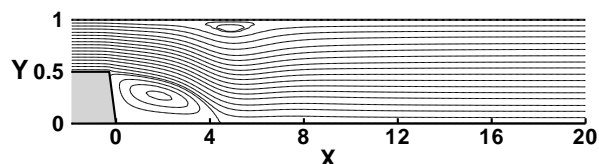


Fig. 7 Distribution of streamlines contours, $\text{Re} = 500$, $\phi = 60^\circ$

In order to illustrate the radiation effect in thermal behaviour of convection flow over an inclined BFS, the isotherms are shown in Figure 8 for three medium situations: 1) pure convection, 2) coupled radiation and forced convection with non-gray gases, and, 3) coupled radiation and forced convection with gray gases. The non-gray medium is considered the real case and the results of other cases will be compared with this real one. In three medium situations, the effect of sudden expansion along the duct is clearly seen from the curvatures of isotherms.

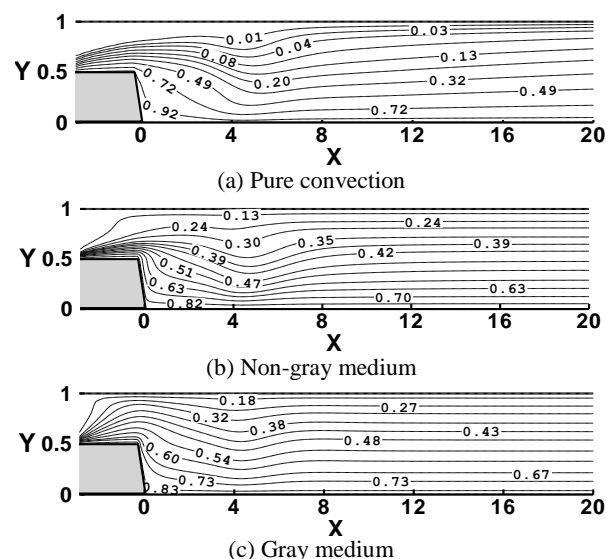


Fig. 8 Distribution of isotherms contours, $\text{RC} = 35$, $\sigma_s = 0$, $\epsilon_w = 0.8$

The effects of radiation on temperature distribution can be found if one compares Figure 8(a), (b) and (c) with each other.

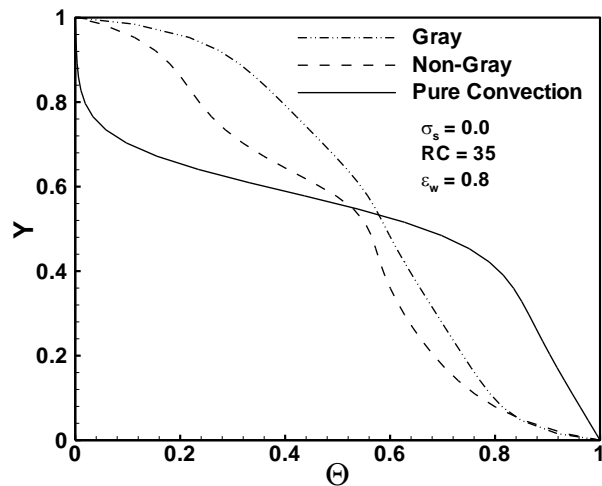
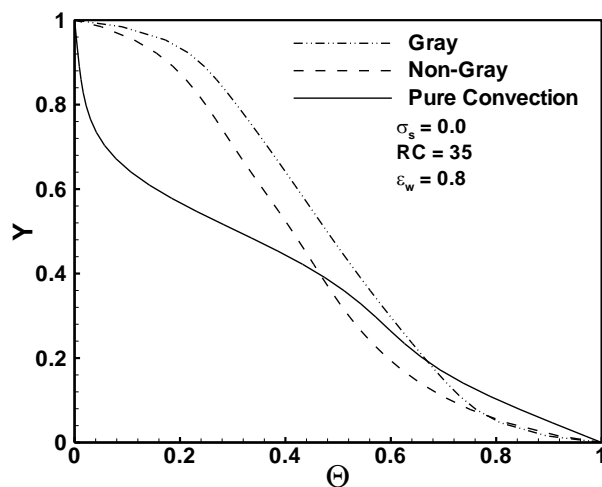
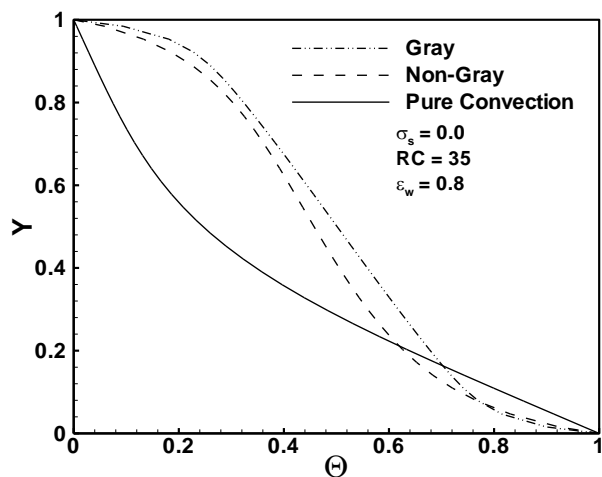
(a) $X=0.5$ (b) $X=3.0$ (c) $X=14.5$

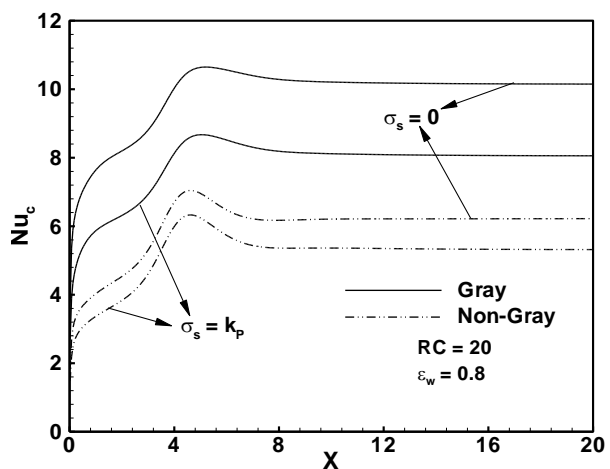
Fig. 9 Temperature distributions along y-axis at three different locations of X

As it is seen from Figure 8, the radiation makes the isotherms more homogenous in comparison with the temperature distribution in the pure convection situation. Moreover, the effect of radiation is seen obviously from the temperature gradients near the step and top walls, which are high because of radiative heat flux. Also, Figure 8 shows that the medium with gray assumption reaches to the thermal fully developed condition at a shorter distance from the entrance, whereas in the pure convection situation, this condition occurs at a larger distance. In order to show the thermal pattern in duct more clearly, the temperature distributions along y-axis is plotted in Figure 9 at three different locations of X. This figure shows the same behaviour for the convective flow as it was seen before in Figure 8.

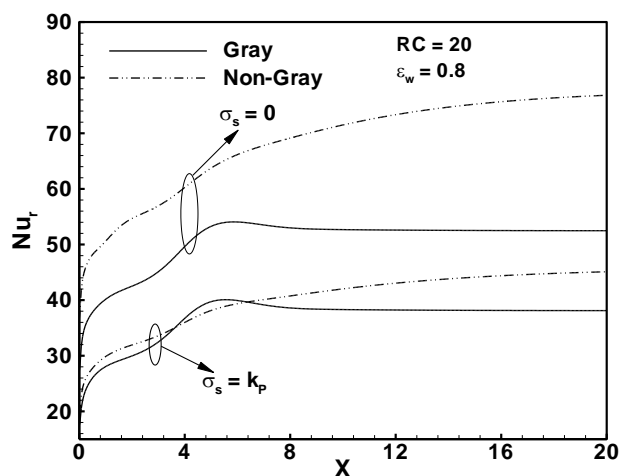
However, Figures 8 and 9 show different results for different medium assumptions, such that none of the assumptions are near the real situation (non-gray medium). Specially, the results of the pure convection are very far from the real case; therefore, neglecting the radiation part in calculations is not acceptable. In the next tables and figures, an attempt is made to study the effect of radiative parameters on the thermal behaviours of the radiative-convective systems in both gray and non-gray mediums. Distributions of convective, radiative and total Nusselt numbers along the bottom wall are shown in Figure 10 for gray and non-gray mediums with and without considering the scattering effects. A same trend is seen from Figure 10(a) for the variations of Nu_c in different mediums. This figure presents that the minimum value of Nu_c occurs on the bottom wall at the backward step corner, where the fluid is at rest.

Also, it is seen that downstream the step location, the Nu_c increases sharply in the primary recirculation region because of the flow vortices, such that its maximum value occurs near the reattachment point. Then, the Nu_c decreases and approaches to a constant value as the distance continues to increase in the stream-wise direction. It should be noted that this constant value for Nusselt number is due to the fully developed condition.

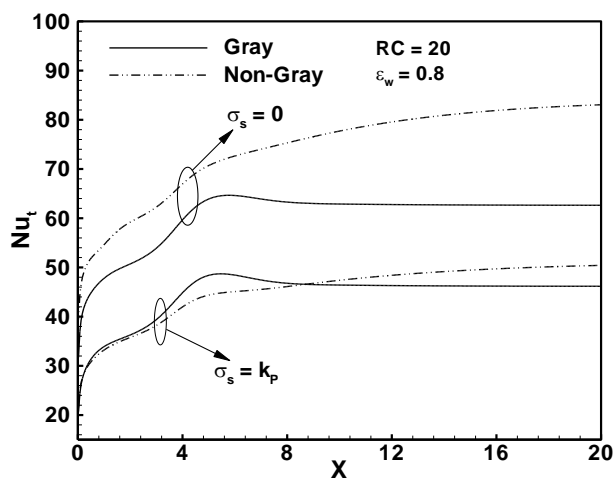
But as it is seen from Figure 10(b), the trend of Nu_r distribution in the gray medium is slightly different from the non-gray medium. In the gray medium, the Nu_r starts from a minimum value at the step corner where the minimum radiative heat flux leaves the bottom wall. Then, as the distance increases from the step corner, the amount of radiative heat flux and consequently Nu_r increases sharply and reaches to a peak, which is due to a decrease in bottom wall incident radiative heat flux incoming from the step surface.



(a) Convective Nusselt number



(b) Radiative Nusselt number



(c) Total Nusselt number

Fig. 10 Distributions of Nusselt numbers along the bottom wall for different mediums

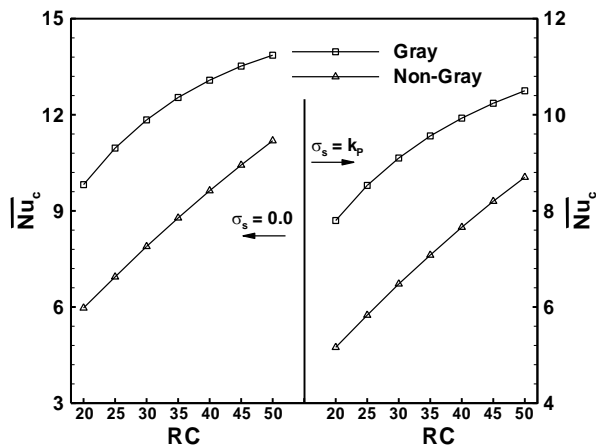
After this peak, the Nu_r decreases and reaches to a constant value as the distance continues to increase in the stream-wise direction. But in the non-gray medium, downstream the step location, the Nu_r always increases until it reaches to a constant value and there is not any peak in distribution of the radiative Nusselt number. Comparison of convective Nusselt number distribution in Figure 10(a) with Nu_r distribution shown in Figure 10(b) illustrates that the values of Nu_r are larger in comparison with Nu_c ; therefore, the trend of total Nusselt number distribution is almost similar to Nu_r , as seen in Figure 10 (c).

According to Figure 10(a), distribution of convective Nusselt number shows different results for gray and non-gray mediums regardless of scattering and non-scattering radiation. This figure shows that the gray assumption leads to wrong results in computing the value of convective Nusselt number. Figures 10(b) and (c) show that in the scattering medium, distribution of Nu_r and consequently Nu_t for gray and non-gray mediums are relatively close to each other. While in the non-scattering medium, these variables for two mentioned medium are far from each other.

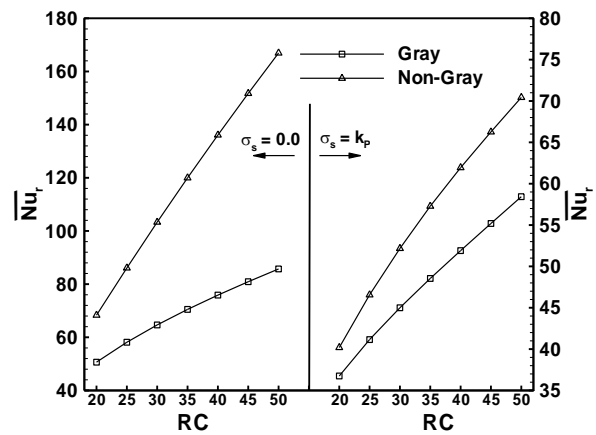
Moreover, Figures 10(a) to (c) illustrate that in the case of having participating medium with scattering effect, the rate of heat transfer from the heated walls into convection flow decreases. Therefore, the amounts of Nusselt numbers in non-scattering medium are larger in comparison with scattering one. In order to have a better comparison between the results in the gray and non-gray simulations, the average convective, radiative and total Nusselt numbers ($\overline{Nu} = \frac{1}{L_2} \int_0^{L_2} Nu dx$) along

the bottom wall at different RC parameters ($20 \leq RC \leq 50$) are presented in Figure 11.

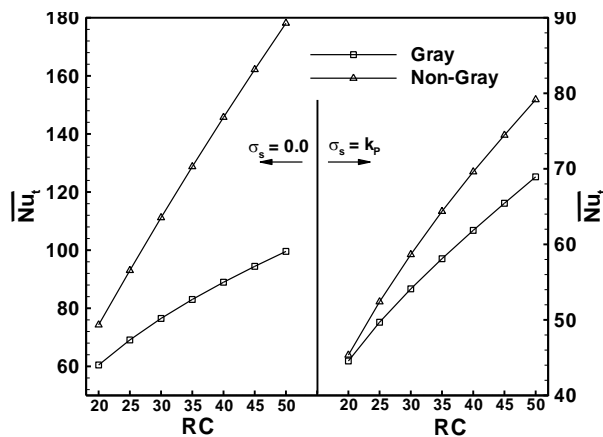
Radiation-conduction parameter (RC) is one of the main parameters in the combined radiation-conduction systems, which shows the relative importance of the radiation mechanism compared with its conduction counterpart. High value of RC parameter shows the radiation dominance in a thermal system. It can be concluded from Figures 11(a) to (c) that the RC parameter has a significant effect in the average convective, radiative and total Nusselt numbers in both gray and non-gray mediums. These figures show that increasing in RC parameter leads to a considerable increase in the average Nusselt numbers, which is due to the significant increase in bottom wall's outgoing radiative and convective heat fluxes. It can be found from Figure 11(a) that in both scattering and non-scattering mediums, the results of $\overline{Nu_c}$ for gray medium are different from the non-gray one.



(a) Average convective Nusselt number



(b) Average radiative Nusselt number



(c) Average total Nusselt number

Fig. 11 Effect of RC on the average Nusselt numbers along the bottom wall in different mediums

Therefore, the gray medium assumption leads to large errors in calculating of $\overline{Nu_c}$, especially at low values of RC. This is due to this fact that in the medium with

gray assumption, the absorption coefficient is constant for all wavenumbers and it is an average value of the whole spectrum (Planck-mean absorption coefficient). But, in the non-gray medium, the absorption coefficient changes with the wavenumbers and in most of the spectrum is zero or near zero, as it is seen from Figure 2. Therefore, these behaviours of absorption coefficient causes that the temperature field and consequently convective Nusselt number in gray medium become different from non-gray one.

In order to show more clearly the difference between gray and non-gray behaviours, the amount of error in computing the average convective Nusselt numbers along the bottom wall in gray and non-gray mediums

$$\left(\frac{(\overline{Nu_c})_{non-gray} - (\overline{Nu_c})_{gray}}{(\overline{Nu_c})_{non-gray}} \right)$$

are tabulated in Table 4.

Table 4 The difference between the average convective Nusselt number in gray and non-gray mediums

$$\left(\frac{(\overline{Nu_c})_{non-gray} - (\overline{Nu_c})_{gray}}{(\overline{Nu_c})_{non-gray}} \right), \epsilon_w = 0.8$$

RC	Difference (%) in non-scattering medium ($\sigma_s = 0$)	Difference (%) in scattering medium ($\sigma_s = k_p$)
20	64.49	51.16
25	57.92	46.31
30	50.06	40.43
35	42.82	35.02
40	35.82	29.63
45	29.62	24.87
50	23.86	20.69

As it is seen from this table, by increasing in the RC parameter, difference between gray and non-gray assumptions in computing the $\overline{Nu_c}$ decreases, such that the highest error rate occurs at lowest value of RC. Furthermore, Table 4 demonstrates that the amount of difference between gray and non-gray cases in scattering medium is less in comparison to the non-scattering medium. But a different trend is seen from Figure 11(b) for the difference between the $\overline{Nu_r}$ in the gray and non-gray mediums with RC parameter. This figure shows that the amount of difference between gray and non-gray assumptions in calculating the values of $\overline{Nu_r}$ increases by increase in the RC parameters.

In principle, these differences are much more for non-scattering medium. For better explanation of these results, Table 5 is presented. According to this table, if

one compares the presented results for non-scattering medium with those tabulated for scattering medium, it can be concluded that in the absence of scattering, the effects of RC parameter on difference between gray and non-gray mediums is greater in comparison to the scattering medium. Besides, Table 5 clearly shows that in the non-scattering case, the gray results are far from real case. Therefore, the gray calculations cannot predict the real behaviour of participating medium.

Table 5 The difference between the average radiative Nusselt number in gray and non-gray mediums

$$\left(\frac{(\overline{Nu_r})_{non-gray} - (\overline{Nu_r})_{gray}}{(\overline{Nu_r})_{non-gray}} \right), \epsilon_w = 0.8$$

RC	Difference (%) in non-scattering medium ($\sigma_s = 0$)	Difference (%) in scattering medium ($\sigma_s = k_p$)
20	25.88	8.56
25	32.45	11.61
30	37.42	13.74
35	41.24	15.25
40	44.25	16.19
45	46.68	16.75
50	48.66	17.03

Table 6 Difference between the average total Nusselt number in gray and non-gray mediums

$$\left(\frac{(\overline{Nu_t})_{non-gray} - (\overline{Nu_t})_{gray}}{(\overline{Nu_t})_{non-gray}} \right), \epsilon_w = 0.8$$

RC	Difference (%) in non-scattering medium ($\sigma_s = 0$)	Difference (%) in scattering medium ($\sigma_s = k_p$)
20	18.60	1.74
25	25.70	5.17
30	31.20	7.74
35	35.51	9.73
40	38.96	11.15
45	41.77	12.11
50	44.02	12.91

Originally, overall thermal behaviours of the convective-radiative system can be determined by total Nusslet number. As it is seen from Figure 11(c), trend of $\overline{Nu_t}$ is almost similar to $\overline{Nu_r}$, which is due to the

large amounts of $\overline{Nu_r}$ in compared to the $\overline{Nu_c}$. However, in order to have a comprehensive comparison between the results of gray medium situation and non-gray one, Table 6 is presented. This table clearly indicates that a significant mistake is made by assuming the gray medium in heat transfer analysis of the non-scattering medium, especially at high values of RC. But, in the scattering medium, the amounts $\overline{Nu_t}$ for the gray medium assumption are close to the non-gray results. Therefore, gray medium assumption gives acceptable results in calculating $\overline{Nu_t}$ for the scattering medium, especially at low values of RC.

In convection-radiation systems, the wall emissivity (ϵ_w) is one of the main factors in controlling the rate of heat transfer. The effects of this parameter on the average convective, radiative and total Nusselt numbers at the bottom wall are presented in Figures 12(a) to (c), respectively. According to Figure 12(a), it can be concluded that the wall emissivity has a considerable effect on $\overline{Nu_c}$, such that increasing in this parameter leads to decrease in $\overline{Nu_c}$. This is due to this fact that under the effective presence of radiation mechanism at high values of wall emissivity, the temperature gradient on the heated walls decreases that leads to decrease in convective Nusselt number.

Also, this figure clearly shows that in both scattering and non-scattering mediums, wall emissivity has more effect on $\overline{Nu_c}$ in the gray medium. In fact, in computing $\overline{Nu_c}$, the gray assumption overestimates the value of this parameter, especially at low values of wall emissivity.

Comparison of $\overline{Nu_c}$ in Figure 12(a) with $\overline{Nu_r}$ shown in Figure 12(b) demonstrates that the wall emissivity has opposite effects on $\overline{Nu_r}$ in comparison with $\overline{Nu_c}$. As it is clear from Figure 12(b), the $\overline{Nu_r}$ increases by increasing in wall emissivity, which is due to the increase in bottom wall's outgoing radiative heat flux in radiation dominance condition. Another interesting behavior in Figure 12(b) is that for low wall emissivity ($0 \leq \epsilon_w \leq 0.2$), the $\overline{Nu_r}$ variations in the gray medium are identical with the results obtained from non-gray one, while for other values of wall emissivity, the gray assumption underestimates the value of radiative Nusselt number, especially at black walls.

It is necessary to note that in scattering medium, the effects of wall emissivity on difference between the $\overline{Nu_r}$ in the gray and non-gray mediums is less in comparison to the non-scattering one. As it is seen from Figure 12(c), the $\overline{Nu_t}$ like the $\overline{Nu_r}$ increases by

increasing the values of wall emissivity. Finally, it should be mentioned that the difference between gray and non-gray assumptions in computing \overline{Nu}_t is very dependent on the wall emissivity and scattering process which can be seen obviously in Figure 12(c).

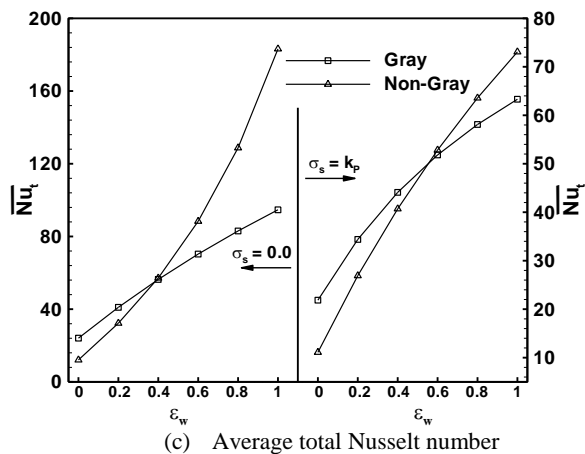
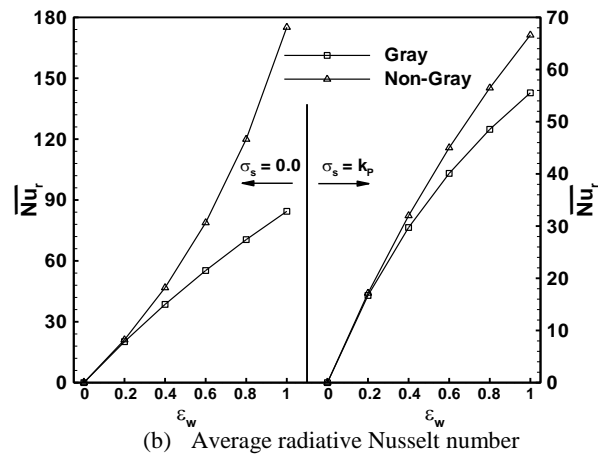
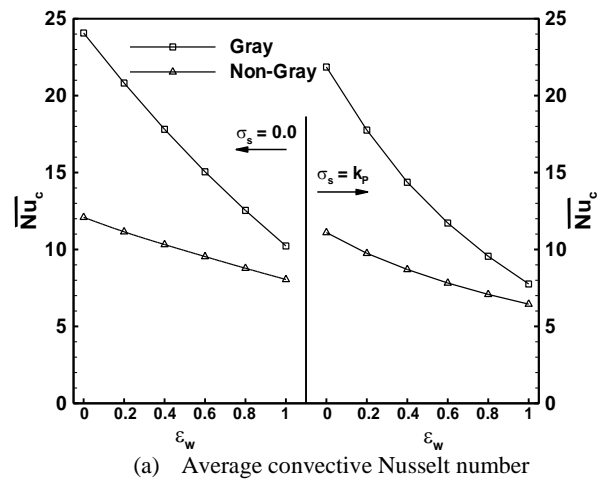


Fig. 12 The effect of wall emissivity on the average Nusselt numbers along the bottom wall in different mediums

7 CONCLUSION

The interaction between non-gray radiation and forced convection in a laminar radiating gas flow over an inclined backward facing step has been investigated in the present work. The full-spectrum k-distribution method (FSK) is used to account for non-gray radiation properties, while the gray radiation calculations are done using the Planck mean absorption coefficient. The continuity, momentum, and energy equations are solved numerically by the CFD techniques in the Cartesian coordinate system using the blocked-off method. To calculate the radiative term in the energy equation, the RTE is solved by the DOM to obtain the distribution of radiant intensity inside the radiating medium. The effects of radiation-conduction parameter, wall emissivity and scattering coefficient on thermal behaviors of the convection-radiation system are thoroughly explored for both gray and non-gray medium situations. In addition, the results of gray medium are compared with non-gray results as a real case. This comparison illustrates that the difference between gray and non-gray mediums is intensively dependent on the radiative parameters, such that in many cases, the gray medium assumption leads to wrong results.

8 NOMENCLATURE

a	Weight function for full-spectrum k-distribution method
c_p	Specific heat, (J.Kg ⁻¹ .K ⁻¹)
ER	Expansion ratio
f	k-distribution, (m)
g	Cumulative k-distribution
I	Radiation intensity, (W.m ⁻²)
k	Absorption coefficient variable (m ⁻¹)
k_p	Planck-mean absorption coefficient (m ⁻¹)
Nu_c	Convective Nusselt number
\overline{Nu}_c	Average convective Nusselt number
Nu_r	Radiative Nusselt number
\overline{Nu}_r	Average radiative Nusselt number
Nu_t	Total Nusselt number
\overline{Nu}_t	Average total Nusselt number
q_c	Convective heat flux, (W.m ⁻²)
q_r	Radiative heat flux, (W.m ⁻²)
q_t	Total heat flux, (W.m ⁻²)
Re	Reynolds number
RC	Radiation-conduction parameter
s	Height of step, (m)
T	Temperature, (K)

T_{ave}	Average temperature, (K)
U_o	Average velocity of the incoming flow at the inlet section (m/s)
u, v	x- and y-components of velocity, (m/s)
U, V	Dimensionless x- and y-component of velocity
x, y	Horizontal and vertical distance, respectively,
X, Y	Dimensionless horizontal and vertical coordinate, respectively
x_r	Reattachment length (m)

Greek Symbols

α	Thermal diffusivity, ($m^2.s^{-1}$)
σ	Stefan Boatsman's constant = 5.67×10^{-8} , ($W.m^{-2}.k^{-4}$)
$\sigma_{a\eta}$	Spectral absorbing coefficient, (m^{-1})
σ_s	Scattering coefficient, (m^{-1})
ε	Wall emissivity
ϕ	Step inclination angle
κ	Thermal conductivity
μ	Dynamic viscosity ($N.s/m^2$)
ρ	Density (kg/m^3)
Θ	Dimensionless temperature
Θ_b	Mean bulk temperature
θ_1, θ_2	Dimensionless temperature parameters
η	Wavenumber, (cm^{-1})

Subscripts

b	Black body
c	Convective, or cold wall
g	Cumulative k-distribution
h	Hot wall
in	Inlet section
r	Radiative
t	Total
w	Wall
η	Wavenumber, (cm^{-1})

REFERENCES

- [1] Armaly, B. F., Durst, F., Pereira JCF, and Chonung, B., "Experimental and Theoretical Investigation of Backward-Facing Step Flow", *Journal of Fluid Mechanics*, Vol. 127, 1983, pp. 473-496.
- [2] Iwai, H., Nakabe, K., and Suzuki, K., "Flow and Heat Transfer Characteristics of Backward-Facing Step Laminar Flow in a Rectangular Duct", *International Journal of Heat and Mass Transfer*, Vol. 43, 2000, pp. 457-471.
- [3] Tylli, N., Kaiktsis L., and Ineichen, B., "Side Wall Effects in Flow Over Backward-Facing Step: Experiments and Numerical Solutions", *Physics Fluids*, Vol. 14, No. 11, 2002, pp. 3835-3845.
- [4] Abu-Mulaweh, H. I., "A Review of Research on Laminar Mixed Convection Flow Over Backward- and Forward-Facing Steps", *International Journal of Thermal Sciences*, Vol. 42, 2003, pp. 897-909.
- [5] Erturk, E., "Numerical Solutions of 2-D Steady Incompressible Flow Over a Backward-Facing Step, Part I: High Reynolds Number Solutions", *Computers & Fluids*, Vol. 37, 2008, pp. 633-655.
- [6] Atashafrooz, M., Gandjalikhan Nassab, S. A. and Ansari, A. B., "Numerical Analysis of Laminar Forced Convection Flow Over Backward and Forward Facing Steps in a Duct Under Bleeding Condition", *International Review of Mechanical Engineering*, Vol. 5, No. 3, 2011, pp. 513-518.
- [7] Nie, J.H., Chen Y.T., and Hsieh, H.T., "Effects of a Baffle on Separated Convection Flow Adjacent to Backward-Facing Step", *International Journal of Thermal Sciences*, Vol. 48, 2009, pp. 618-625.
- [8] Tsay, Y. L., Chang T. S., and Cheng, J. C., "Heat Transfer Enhancement of Backward-Facing Step Flow in a Channel by Using Baffle Installation on Channel Wall", *ACTA Mechanica*, Vol. 174, 2005, pp. 63-76.
- [9] Chen, Y. T., Nie, J. H., Hsieh, H. T., and Sun, L.J., "Three-Dimensional Convection Flow Adjacent to Inclined Backward-Facing Step", *International Journal of Heat and Mass Transfer*, Vol. 49, 2006, pp. 4795-4803.
- [10] Abu-Nada, E., "Investigation of Entropy Generation Over a Backward Facing Step Under Bleeding Conditions", *Energy Conversion and Management*, Vol. 49, 2008, pp. 3237-3242.
- [11] Atashafrooz, M., Gandjalikhan Nassab, S. A., and Ansari, A. B., "Numerical Study of Entropy Generation in Laminar Forced Convection Flow Over Inclined Backward and Forward Facing Steps in a Duct", *International Review of Mechanical Engineering*, Vol. 5, No. 5, 2011, pp. 898-907.
- [12] Atashafrooz, M., Gandjalikhan Nassab S. A., and Ansari, A. B., "Numerical Investigation of Entropy Generation in Laminar Forced Convection Flow Over Inclined Backward and Forward Facing Steps in a Duct Under Bleeding Condition", *Thermal Science*, Vol. 18, No. 2, 2014, pp. 479-492.
- [13] Selimefendigil, F., and Oztop, H. F., "Numerical Analysis of Laminar Pulsating Flow at a Backward Facing Step with an Upper Wall Mounted Adiabatic Thin Fin", *Computers & Fluids*, Vol. 88, 2013, pp. 93-107.
- [14] Selimefendigil, F., Oztop, H. F., "Effect of a Rotating Cylinder in Forced Convection of Ferrofluid Over a Backward Facing Step", *International Journal of Heat and Mass Transfer*, Vol. 71, 2014, pp. 142-148.
- [15] Yan W. M., Li, H.Y., "Radiation Effects on Mixed Convection Heat Transfer in a Vertical Square Duct", *International Journal of Heat and Mass Transfer*, Vol. 44, 2001, pp. 1401-1410.
- [16] Chiu, H. C., Jang, J. H., and Yan, W. M., "Mixed Convection Heat Transfer in Horizontal Rectangular Ducts with Radiation Effects", *International Journal of Heat and Mass Transfer*, Vol. 50, 2007, pp. 2874-2882.
- [17] Chiu, H. C., Yan, W. M., "Mixed Convection Heat Transfer in Inclined Rectangular Ducts with Radiation Effects", *International Journal of Heat and Mass Transfer*, Vol. 51, 2008, pp. 1085-1094.
- [18] Nouanegue, H., Muftuoglu A., and Bilgen, E., "Conjugate Heat Transfer by Natural Convection, Conduction and Radiation in Open Cavities", *International Journal of Heat and Mass Transfer*, Vol. 51, 2008, pp. 6054-6062.

- [19] Ko M., Anand, N. K., “Three-Dimensional Combined Convective-Radiative Heat Transfer Over a Horizontal Backward-Facing Step—A Finite-Volume Method”, *Numerical Heat Transfer, Part A*, Vol. 54, 2008, pp. 109-129.
- [20] Ansari, A. B., Gandjalikhan Nassab, S. A., “Forced Convection of Radiating Gas Over an Inclined Backward Facing Step Using the Blocked-Off Method”, *Thermal Science*, Vol. 17, No. 3, 2013, pp. 773-786.
- [21] Atashafrooz, M., Gandjalikhan Nassab, S. A., “Simulation of Three-Dimensional Laminar Forced Convection Flow of a Radiating Gas Over an Inclined Backward-Facing Step in a Duct Under Bleeding Condition”, *Institution of Mechanical Engineers, Part C, Journal of Mechanical Engineering Science*, Vol. 227, No. 2, 2012, pp. 332-345.
- [22] Atashafrooz, M., Gandjalikhan Nassab, S. A., “Three Dimensional Laminar Convection Flow of Radiating Gas Over a Backward Facing Step in a Duct”, *International Journal of Engineering-Transactions A: Basics*, Vol. 25, No. 4, 2012, pp. 399-410.
- [23] Atashafrooz M., Gandjalikhan Nassab, S. A., “Simulation of Laminar Mixed Convection Recess Flow Combined with Radiation Heat Transfer”, *Iranian Journal of Science and Technology*, Vol. 37, No. M1, 2013, pp 71-75.
- [24] Atashafrooz, M., Gandjalikhan Nassab, S. A., “Combined Heat Transfer of Radiation and Forced Convection Flow of Participating Gases in a Three-Dimensional Recess”, *Journal of Mechanical Science and Technology*, Vol. 26, No. 10, 2012, pp. 3357-3368.
- [25] Farias, T. L., Carvalho, M. G., “Radiative Heat Transfer in Soot-Containing Combustion Systems with Aggregation”, *International Journal of Heat and Mass Transfer*, Vol. 41, 1998, pp. 2581-2587.
- [26] Solovjov, V. P., Webb, B. W., “The Cumulative Wavenumber Method for Modeling Radiative Transfer in Gas Mixtures with Soot”, *Journal of Quantitative Spectroscopy and Radiative Transfer*, Vol. 93, 2005, pp. 273-287.
- [27] Ludwig, C. B., Malkmus, W., Reardon, J. E., and Thomson, J. A. L., “Handbook of Infrared Radiation from Combustion Gases”, *Technical Report SP-3080*, NASA, 1973.
- [28] Edwards, D. K., Balakrishnan, A., “Thermal Radiation by Combustion Gases”, *International Journal of Heat and Mass Transfer*, Vol. 16, No. 1, 1973, pp. 25-40.
- [29] Edwards, D. K., “Molecular Gas Band Radiation,” *Advances in Heat Transfer*, Vol. 12, 1976, pp. 115-193.
- [30] Liu, F., Smallwood, G. J., “An Efficient Approach for the Implementation of the SNB Based Correlated-k Method and Its Evaluation”, *Journal of Quantitative Spectroscopy and Radiative Transfer*, Vol. 84, No. 4, 2004, pp. 465-75.
- [31] Modest, M. F., “Narrow Band and Full Spectrum k-Distributions for Radiative Heat Transfer-Correlated-k vs., Scaling Approximation”, *Journal of Quantitative Spectroscopy and Radiative Transfer*, Vol. 76, No. 1, 2003, pp. 69-83.
- [32] Denison M. K., Webb, B. W., “A Spectral Line Based Weighted Sum of Gray Gases Model for Arbitrary RTE Solvers”, *ASME, Journal of Heat Transfer*, Vol. 115, No. 4, 1993, pp.1004-1012.
- [33] Solovjov, V. P., Webb, B. W., “SLW Modeling of Radiative Transfer in Multi Component Gas Mixtures”, *Journal of Quantitative Spectroscopy and Radiative Transfer*, Vol. 65, 2000, pp. 655-672.
- [34] Modest, M. F., “Radiative Heat Transfer”, 2nd Edition, McGraw-Hill, New York, 2003.
- [35] Pierrot, L., Soufiani, A., and Taine, J., “Accuracy of Narrow-Band and Global Models for Radiative Transfer in H₂O, CO₂, and H₂O-CO₂ Mixtures at High Temperature”, *Journal of Quantitative Spectroscopy and Radiative Transfer*, Vol. 62, 1999, pp. 523-548.
- [36] Colomer, G., Consul, R., and Oliva, A., “Coupled Radiation and Natural Convection: Different Approaches of the SLW Model for a Non-Gray Gas Mixture”, *Journal of Quantitative Spectroscopy and Radiative Transfer*, Vol. 107, 2007, pp. 30-46.
- [37] Ibrahim, A., Lemonnier, D., “Numerical Study of Coupled Double-Diffusive Natural Convection and Radiation in a Square Cavity Filled with A N₂-CO₂ Mixture”, *International Communications in Heat and Mass Transfer*, Vol. 36, 2009, pp. 197-202.
- [38] Modest, M. F., Zhang, H., “The Full-Spectrum Correlated-k Distribution for Thermal Radiation from Molecular Gas-Particulate Mixtures”, *ASME, Journal of Heat Transfer*, Vol. 124, No. 1, 2002, pp. 30-38.
- [39] Tencer, J., Howell, J. R., “A Multi-Source Full Spectrum k-Distribution Method for 1-D Inhomogeneous Media”, *Journal of Quantitative Spectroscopy and Radiative Transfer*, Vol. 129, 2013, pp. 308-315.
- [40] Proter, R., Liu, F., Pourkashanian, M., Williams A., and Smith, D., “Evaluation of Solution Method for Radiative Heat Transfer in Gaseous Oxy-Fuel Combustion Environments”, *Journal of Quantitative Spectroscopy & Radiative Transfer*, Vol. 111, 2010, pp. 2084-2094.
- [41] Lari, K., Baneshi, M., Gandjalikhan Nassab, S. A., Komiya, A., and Maruyama, S., “Numerical Study of Non-Gray Radiation and Natural Convection Using the Full-Spectrum k-Distribution Method”, *Numerical Heat Transfer, Part A*, Vol. 61, 2012, pp. 61-84.
- [42] Atashafrooz M., Gandjalikhan Nassab, S. A., “Numerical Analysis of Laminar Forced Convection Recess Flow with Two Inclined Steps Considering Gas Radiation Effect”, *Computers & Fluids*, Vol. 66, 2012, pp. 167-176.
- [43] Patankar, S. V., Spalding, D. B., “A Calculation Procedure for Heat, Mass and Momentum Transfer in Three-Dimensional Parabolic Flows”, *International Journal of Heat and Mass Transfer*, Vol. 15, No. 10, 1972, pp. 1787-1806.
- [44] Rothman, L. S, et al., “The HITRAN 2008 Molecular Spectroscopic Database”, *Journal of Quantitative Spectroscopy & Radiative Transfer*, Vol. 110, 2009, pp. 533-572.
- [45] Patankar, S. V., “Numerical Heat Transfer and Fluid Flow”, Taylor & Francis, Philadelphia, PA, 1981, Chaps. 7.
- [46] Atashafrooz, M., Gandjalikhan Nassab, S. A., and Sadat Behineh, E., “Effects of Baffle on Separated Convection Step Flow of Radiating Gas in a Duct”, *International Journal of Advanced Design and Manufacturing Technology*, Vol. 8, No. 3, 2015, pp. 33-47.